J Mater Sci (2010) 45:4813–4821
DOI 10.1007/s10853-010-4511-7

ULTRAFINE GRAINED MATERIALS

On the fatigue crack growth–microstructure relationship in ultrafine-grained interstitial-free steel

T. Niendorf · F. Rubitschek · H. J. Maier · D. Canadinc · I. Karaman

Received: 3 February 2010 / Accepted: 9 April 2010 / Published online: 27 April 2010

Abstract The crack growth behavior in an ultrafine-grained (UFG) interstitial-free (IF) steel processed by equal channel angular pressing (ECAP) was investigated utilizing miniaturized compact-tension specimens with different microstructural characteristics. The current results demonstrate that both the ECAP processing route and the direction of crack growth with respect to the extrusion direction dictate the crack growth behavior in UFG IF steel. Specifically, the highest crack growth rates and the lowest threshold values were observed for the lowest grain size. Moreover, an unusual deviation from the expected direction of crack expansion was observed, where the deviation depended on the processing route and direction of crack growth. This deviation is attributed to the presence of elongated structures in the microstructure, which were mainly detectable in the UFG IF steel following a small number of pressings, and to a smaller extent in the optimized microstructures. Specifically, these elongated structures formed parallel to the material's plastic flow during ECAP processing and moved the crack away from the expected direction of growth due to the high stress concentration zones they created along with the process-induced damages.

T. Niendorf (✉) · F. Rubitschek · H. J. Maier
Lehrstuhl für Werkstoffkunde (Materials Science), University of Paderborn, 33095 Paderborn, Germany
e-mail: niendorf@mail.uni-paderborn.de

D. Canadinc
Advanced Materials Group, Department of Mechanical Engineering, Koc University, Sariyer, 34450 Istanbul, Turkey

I. Karaman
Department of Mechanical Engineering, Texas A&M University, College Station, TX 77843, USA

Motivation and significance

Recently, ultrafine-grained (UFG) and nano-crystalline (NC) materials have gained remarkable attention due to their extraordinary properties [1–5]. By reducing the grain size into the submicron regime, the strength of both pure metals and alloys can be increased considerably, while the ductility of these materials is preserved [2, 6]. The techniques for achieving NC materials and UFG materials are fundamentally different: "bottom-up" approaches are employed for achieving NC materials with grain sizes less than 100 nm, while UFG materials with grain sizes ranging from 100 nm up to 1 μm are produced by "top–down" techniques [2, 7, 8]. The latter techniques do less suffer from specific process-induced imperfections, such as impurities, and the processing of relatively large quantities of material is feasible [1, 8]. High pressure torsion (HPT) [9], accumulative roll bonding [10], and equal channel angular pressing (ECAP) [1, 2, 7, 11] are the most commonly utilized techniques, which all make use of severe plastic deformation for achieving the high degree of grain refinement [1, 2]. The homogenously deformed volume fraction of material is the highest upon ECAP processing, and a good repeatability is achieved regarding the final grain size and the resulting texture with this process, making it mostly the method of choice for obtaining UFG microstructures [1, 2, 11].

Many of the studies to date focused on the microstructural evolution during ECAP processing and the resulting monotonic properties [1, 2, 11], and results are now available for various materials featuring different microstructural characteristics, including high-purity face-centered cubic (fcc) metals [2, 12], hexagonal closed packed (hcp) biomaterials [13, 14], and body-centered cubic (bcc) steels [15, 16]. However, establishing a deep knowledge of the

materials' monotonic and cyclic deformation response is crucial for any of the envisaged applications, such as medical implants and light-weight automotive components. Consequently, the investigation of fatigue behavior of UFG materials became of interest to many researchers, and in particular, the microstructural evolution in the high-cycle fatigue (HCF) and the low-cycle fatigue (LCF) regimes has been recently studied in detail [14, 16–19].

So far, the contributions of crack initiation and propagation were considered in a collective manner in the analyses of fatigue behavior [16, 18], and there is a limited amount of data on the crack growth behavior of UFG materials in correlation with the microstructure [17]. To the best of the authors' knowledge, no distinction has been made between the crack initiation and crack propagation behavior for bcc UFG materials, with the exception of one study carried out on bcc UFG low-carbon steels [19], where the material was investigated upon being heat treated. However, it has been previously shown that heat treatment has a significant influence on the fatigue properties of UFG interstitial-free (IF) steel [20], and thus, the generalization of the results obtained in [19] to all bcc UFG steels is questionable.

This study was undertaken with this motivation, in order to focus on the crack propagation behavior in UFG alloys with a bcc structure, and the crack growth behavior of a UFG bcc IF steel was investigated in as-ECAP-processed condition. For this purpose, IF steel samples processed through different processing routes, and thus, with different microstructural characteristics were tested. In particular, crack growth rates were determined as a function of stress intensity factor range (ΔK), and the constants of the Paris law were calculated. Mechanical experiments were accompanied by thorough microstructural investigations. The focus was placed on the crack growth–microstructure relationship with an emphasis on the influence of the ECAP shear plane.[1] The current results indicate that the ECAP processing route is a major parameter dictating the crack growth behavior. Specifically, a higher susceptibility to crack growth was observed for UFG IF steel samples that underwent a higher number of ECAP passes. Furthermore, in all UFG microstructures, the cracks grew along elongated grain structures, which were primarily found on the flow plane parallel to the last ECAP shear plane.

[1] Here "inclination plane" which is also denoted as "grain elongation plane" [11] would be a more appropriate term; however, "shear plane" is used instead in this text as it is the commonly utilized terminology in the literature (Figs. 2 and 4).

Experimental procedures

The chemical composition of the IF steel investigated in this study is tabulated in Table 1 [16]. The initial material was received in form of a hot rolled plate with a thickness of 25 mm. For ECAP processing, billets of 25 × 25 × 175 mm^3 were cut by a low-speed band-saw, such that the longitudinal direction of each billet coincided with the rolling direction of the original plate. The billets were ECAP processed at room temperature at a processing speed of 2.5 mm/s. The ECAP die had a 25 × 25 mm^2 channel with a sharp 90° channel cross-section angle, and benefited from the "sliding walls concept" [21]. The IF steel samples were extracted from billets processed along the ECAP routes 2A, 8B$_C$, 8E, and 16E.[2] Coarse-grained (CG) IF steel was also considered in this study for comparison purposes.

Miniature compact tension (CT) specimens were extracted from the ECAP-processed billets similar to those in ASTM standards [23], however, with slightly different dimensions, as presented in Fig. 1. CG IF steel samples of the same dimensions were obtained by heat treatment of 2A material according to [20]. The samples were cut by wire electro-discharge machining (EDM) in such a way that crack growth only took part in the uniformly processed sections of the ECAP billets [22]. The miniature specimens employed do not meet the minimum thickness criterion for the determination of the critical stress intensity factor (K_{Ic}), and thus, the crack growth curves presented in this study do not go beyond the end of the Paris regime, so that linear elastic fracture mechanics was still applicable. In order to allow for the investigation of the role of the microstructural morphology induced by ECAP processing, the specimens were cut parallel to all three side surfaces of the billets, as depicted in the inset of Fig. 2. Following EDM, the surfaces of the CT specimens were mechanically ground down to a grit size of 5 μm, such that the detrimental effects of EDM on the sample surfaces were eliminated. In order to monitor the fatigue-induced changes in the crack wake, some samples were electropolished prior to cyclic loading to ensure the surface quality needed for electron backscatter diffraction (EBSD) analysis. Electropolishing was conducted utilizing a 5% perchloric acid solution under an applied potential of 30 V at −40°C.

The mechanical tests were carried out on a servo-hydraulic load frame at room temperature. For measuring the crack length, the potential drop method [24] was utilized, where the current was limited to 5 A in order to avoid temperature increase in the samples [25]. The potential drops were measured using a voltmeter with nanovolt resolution. Commercial LabView software was

[2] For more information on ECAP processing routes, see [22].

employed to determine the actual crack length from the measured potential drop and to calculate the actual stress intensity factor. Experiments with a constant frequency of 20 Hz were conducted under ΔK control with a positive stress ratio of $R = 0.1$, where the starting load level corresponded to $\Delta K = 18$ MPa$\sqrt{\text{m}}$. Finally, a scanning electron microscope operating at 20 kV equipped with an EBSD detector, a confocal laser scanning microscope (CSM) equipped with a 408 nm violet laser, and a X-Ray diffractometer (XRD) with a Cu–Kα source operated at 40 kV were utilized for microstructural investigation.

Table 1 Chemical composition of the IF steel investigated in this study [16]

Element	Fe	C	S	N	O	Ti	Al
Weight percent	Balance	0.0023	0.0077	0.0018	0.002	0.065	0.05

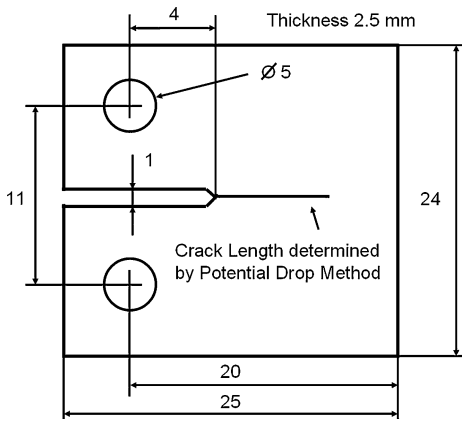

Fig. 1 Geometry of the miniature CT specimens used in this study [25]

Experimental results

The crack growth behavior of the IF steel was strongly dependent on the microstructure, which itself was dictated by the ECAP processing route. Figure 2 depicts crack growth curves of CG and UFG IF steel samples. The crack growth curves shown in Fig. 2 were all obtained on samples extracted parallel to the transverse plane (TP), as shown in the inset of Fig. 2. Obviously, crack growth rates increased and fatigue threshold values (ΔK_{th}) decreased in the following order: CG, 2A, 8E, 16E and finally $8B_C$. The threshold value for the CG IF steel was 9.5 MPa$\sqrt{\text{m}}$, whereas ΔK_{th} for the UFG IF steel from route-$8B_C$ was 5.0 MPa$\sqrt{\text{m}}$. Differences in crack growth behavior were pronounced in the near-threshold region, while in the Paris regime the behavior of IF steel samples with different microstructures was rather similar. Thus, the same Paris law constants were assigned within this region for all UFG IF steel samples: $C = 7.5 \times 10^{-11}$ m/cycle, $m = 2.3$. The inset shown in the right lower corner of Fig. 2 schematically depicts the variation in crack growth direction for different IF steel samples. Crack growth perpendicular to the loading direction was observed for CG IF steel and

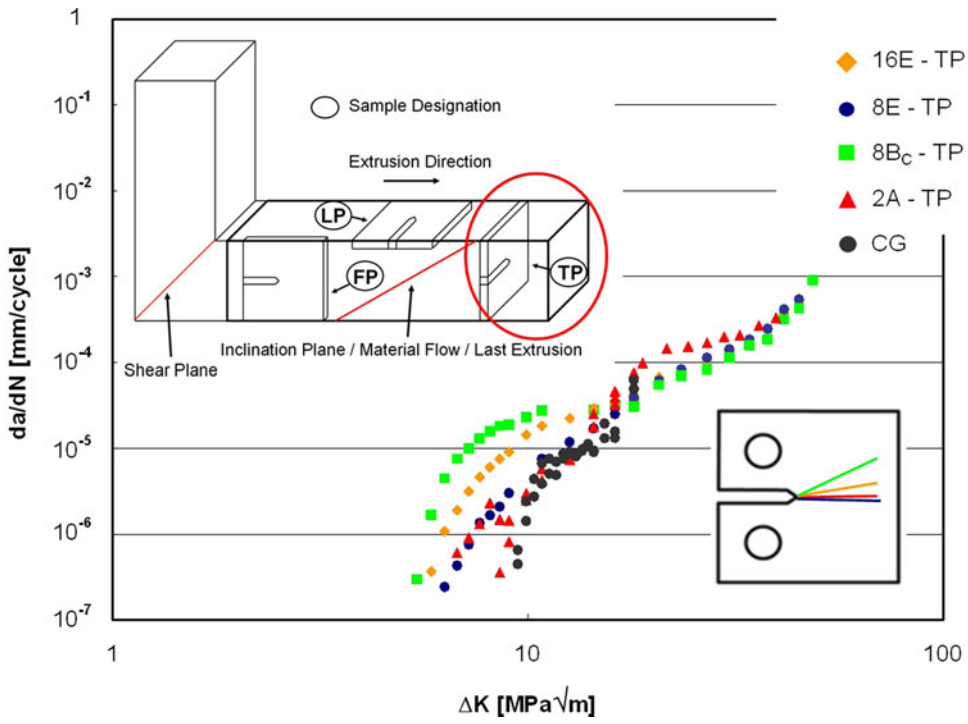

Fig. 2 Crack growth rates as a function of ΔK for UFG steel samples extracted parallel to TP. The insets depict the sample orientation and the direction of crack growth for different TP IF steel microstructures

UFG IF steel samples processed along routes 2A and 8E, and deviations from this normal crack growth direction were noted in the case of route-16E- and $8B_C$-processed UFG IF steel samples. For the latter UFG condition a maximum deviation of about 30° from the normal crack growth direction was observed, which has to be considered in the evaluation of the measured crack growth rates, as will be discussed later in this paper.

The SEM micrographs shown in Fig. 3 depict the cracks grown in UFG IF steel samples with different microstructures at various stages of fatigue. Obviously, crack growth direction differs already in the very early stages directly after crack initiation from the notch. The crack growth is very similar in route-2A and 8E UFG IF steels, i.e., perpendicular to the loading direction. No pronounced differences are visible, but for the given loading conditions (corresponding to $\Delta K = 18$ MPa$\sqrt{\text{m}}$), the crack path in the route-2A UFG IF steel turns out slightly more tortuous. In comparison to these samples, the crack growth behavior in the UFG IF steel samples processed along both ECAP routes 16E and $8B_C$ differs significantly. The crack growth direction is unusual, such that the crack deviates about 10° and 30° from the expected crack growth direction in route-16E and route-$8B_C$ material, respectively. The crack path in both cases is as tortuous as in the case of the route-8E UFG IF steel.

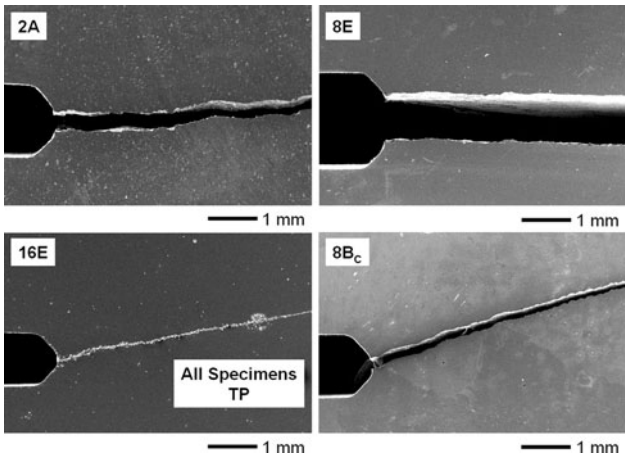

Fig. 3 Micrographs depicting the crack paths in UFG IF steel samples under loading in the vertical direction. Route-2A and 8E materials exhibit normal crack growth, while route-$8B_C$ and 16E materials are characterized by an unusual crack path

In order to examine the influence of the crack growth direction and sample orientation with respect to the extrusion direction and the last ECAP shear plane, a set of crack growth experiments were conducted on route-2A and $8B_C$ UFG IF steel samples. The curves displaying the crack growth behavior on three different planes are presented in Fig. 4. As already shown in Fig. 2, the route-$8B_C$ material is characterized by larger crack growth rates and lower threshold values as compared to the route-2A UFG IF steel. Comparison of the results obtained from the differently oriented samples of the route-2A UFG IF steel yields a significant variation. Threshold values are in the range of 6.8–8.6 MPa$\sqrt{\text{m}}$, and the sample orientation seems to have

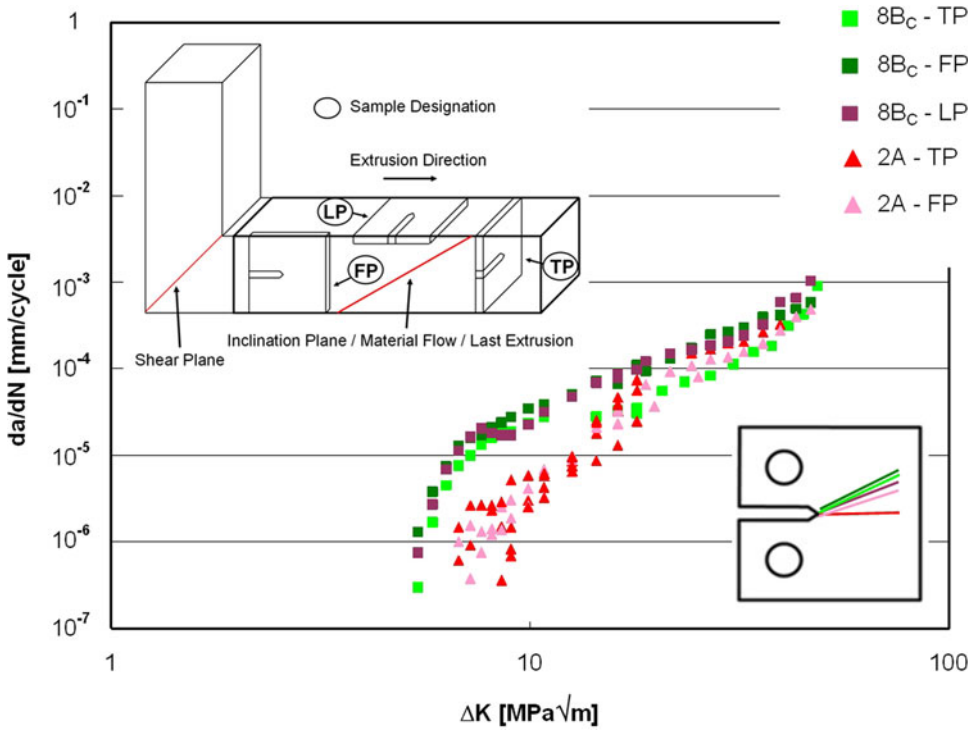

Fig. 4 Crack growth rates as a function of ΔK for UFG steel samples processed along ECAP routes 2A and $8B_C$. The insets depict the different sample orientations with respect to the last ECAP shear plane, and the direction of crack growth for each of the IF steel variants

only a slight influence on this value. But as shown in the inset in the lower right corner of Fig. 4, the growth directions of the cracks on the TP and flow plane (FP) differ significantly: on the TP the crack growth occurs perpendicular to the loading axis, while an offset of about 30° is present on the FP. This, of course, leads to an underestimation of the crack growth rate on the FP (see Discussion for details). Specifically, crack growth takes place almost parallel to the last ECAP shear plane on the FP. For the route-8B_C UFG IF steel on all planes (TP, FP and longitudinal plane (LP)) a similar direction of crack growth is observed, such that even the crack growth rates as a function of ΔK are similar. On FP and LP, crack growth direction can be linked to ECAP shear planes, and it can be correlated to the last ECAP shear plane on FP and to the penultimate shear plane on LP.

In order to investigate the crack growth behavior on a smaller scale, SEM and CSM studies were carried out (Fig. 5). The SEM images show the typical crack growth behavior for the route-8B_C UFG IF steel, and a step-like structure is visible on all surfaces. In general the crack is characterized by the deviation of about 30° from the expected crack growth direction as described above, however; regular small increments are present where the crack propagates along the originally expected direction, which is perpendicular to the loading direction. In addition, kinking bifurcation of the crack is often detectable. As shown in the three-dimensional (3D) surface plot obtained from CSM, the surface of the sample is characterized by a significantly distorted topography when the crack is kinked.

The EBSD grain maps shown in Fig. 6 depict the microstructures of route-2A and 8B_C UFG IF steels in the crack wake on the FP. For the route-2A material it is obvious that crack growth follows elongated structures, which are indeed agglomerations of subgrains only divided by low-angle grain boundaries (LAGBs). Crack advance on these boundaries seems to be very easy, and the crack growth direction changed only when it approached a region characterized by more equiaxed grains separated mainly by high-angle grain boundaries (HAGBs) (upper images in Fig. 6), where a kink evolved. Since the grain refinement in the route-8B_C IF steel is much more effective, all aspects of crack growth were studied on a smaller scale (lower images of Fig. 6). Accordingly, the large elongated structures present in the route-2A material were not present anymore, but still the microstructure consisted of elongated structures, and the crack growth took place parallel to these structures.

Since crack growth is a bulk phenomenon, investigation of the crack growth–microstructure relationship only on the samples' surfaces is not sufficient. Therefore, the crack surfaces of all samples were investigated, as well. Figure 7 displays the crack surface of a route-8B_C CT sample (TP). For better monitoring of the damage on this surface, the angle of view was set at 70°. The crack surface shown in Fig. 7 is very distorted, and a secondary crack parallel to the crack surface and delamination of a large area are visible. The height of the delaminated area is about 25 µm, very well exceeding the average grain size of the route-8B_C UFG IF steel. Such delaminations were present in all UFG IF steel variants regardless of the loading conditions.

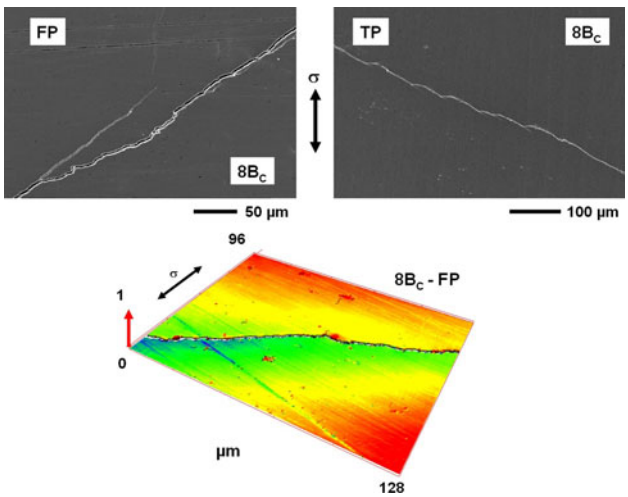

Fig. 5 SEM and CSM micrographs depicting the crack paths in route-8B_C UFG IF steel in differently oriented samples. The SEM micrographs show a step-like crack path at different length scales on both flow and transverse planes. The CSM results indicate increased surface topography in a region where the crack is kinked, the maximum topography shown in the CSM map is 1 µm

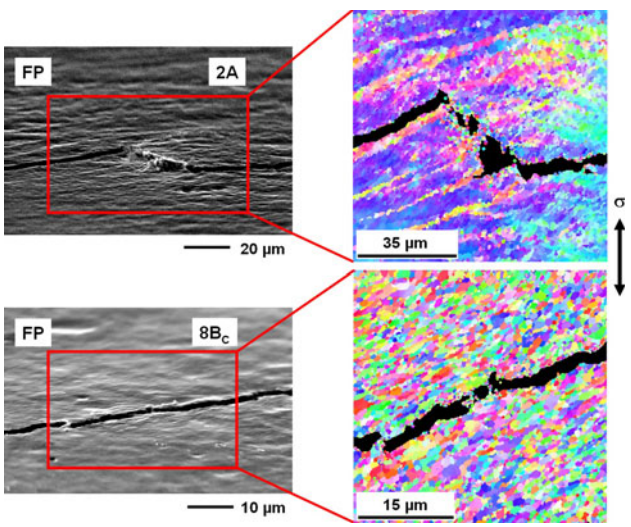

Fig. 6 SEM micrographs (the images are foreshortened as samples are mounted at a 70° angle for EBSD analyses) and the corresponding EBSD grain maps. Both EBSD analyses were carried out on the flow plane. The crack follows the elongated grain structures in both cases

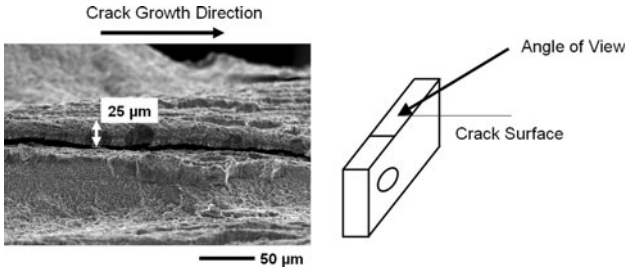

Fig. 7 SEM micrograph displaying the crack surface of a fatigued route-8B_C TP sample. As depicted in the schematic, the micrograph was recorded at an angle of view of about 70°. A secondary crack is visible parallel to the surface and at a distance of 25 µm, which is much larger than the average grain size

Discussion

Sample geometry

In this study, the stage three of the crack growth behavior was not investigated due to the geometry of the miniaturized CT samples, which do not meet the minimum thickness criterion formulated in the former version of the actual ASTM standard. The ligament beyond the phase of stable crack growth is quite small leading to final failure that is mainly characterized by plastic deformation, so failure does not occur in a fracture mechanics manner [25]. However, in the range of ΔK considered in the experiments, the boundary conditions of fracture mechanics testing are fulfilled, i.e., the plastic zone is small with respect to the crack length, the ligament, and the overall sample dimensions. The highest crack growth rates and the lowest threshold value were exhibited by the route-8B_C UFG IF steel, where the crack growth was not perpendicular to the loading direction (Figs. 2 and 3). Consequently, the potential drop method used for the measurement of crack length leads to an underestimation of the crack length, since it primarily detects the resistance of the smallest cross-section of the CT specimen, i.e., the ligament in front of the crack. Eventually, this underestimation of the actual crack length leads to lower crack growth rates. However, both values can be corrected by multiplication with a constant factor, which is defined by the angle of deflection. Since this correction factor is close to one, it was not applied to the results shown in Figs. 2 and 4 in this study.

Fatigue performance and crack propagation

It is interesting to note that crack growth resistance of route-8B_C UFG IF steel, which has been shown to exhibit superior fatigue performance both in the LCF and HCF regimes [16, 20], (Niendorf (2010) Unpublished data) is indeed inferior, based on the current results (Fig. 2). A similar trend was observed for the routes optimized for high strength and superior fatigue performance (16E and 8E), while the crack growth rates were smaller for the non-optimized route (2A) and the CG material. It is well known that total fatigue life can be subdivided into three phases: crack initiation, crack propagation and the final failure of the material. As crack growth rates for the optimized ECAP routes are higher, the superior fatigue lives of the optimized UFG IF steel variants can only be attributed to a significantly longer phase of fatigue crack initiation. Similar results have been shown for other UFG materials, such as copper and aluminum alloys [17, 26–28]. In all cases, the optimized routes exhibited superior fatigue performance yet larger crack growth rates, regardless of the specimen geometry.

Two main reasons have been forwarded to explain the observed phenomenon: the crack paths in UFG materials are less tortuous, and roughness-induced crack closure is not as pronounced as in the CG material. Accordingly, a more tortuous crack path in any material leads to an effectively longer crack path, and eventually to more energy consumption during fatigue crack growth [17, 29, 30]. In the current material, all crack paths seem to be nearly straight (Fig. 3), which has also been observed in UFG IF steel samples of different geometries (Niendorf (2010) Unpublished data). The presence of crack closure mechanisms decreases the range of ΔK with a fully opened crack, which in fact is a prerequisite for crack advance [19, 30–32]. Thus, any mechanism leading to crack closure can slow down crack growth [31, 32].

Crack propagation direction

In order to support the conclusions made in the following paragraphs it is important to characterize the condition of the IF steel prior to ECAP processing. The material investigated was hot rolled and cooled down slowly, permitting a full recrystallization. As it is known from bcc materials this may lead to the evolution of an inherent texture, which could result in failure along specific planes after subsequent deformation processing. Therefore, texture of the CG IF steel prior to ECAP processing has been investigated (Fig. 8). The inverse pole figures shown in Fig. 8 clearly demonstrate that only weak texture is present and texture is not changed significantly upon ECAP processing in case of the IF steel. Thus, initial texture cannot be the reason for the unusual crack propagation directions found.

The current results (Figs. 2 and 3) demonstrate that the crack growth direction on TP in the route-16E and 8B_C UFG IF steel can deviate from the expected one in this case. The ECAP shear plane cannot play a significant role since the ECAP shear plane is not visible on TP. In order to

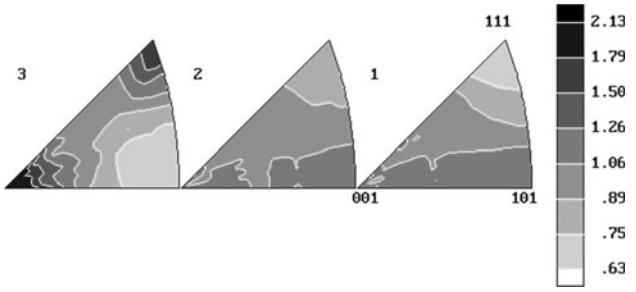

Fig. 8 X-ray diffraction results displaying the texture of IF steel in the as-received (CG) condition

relate crack growth to the last ECAP shear plane, specimens were cut parallel to FP (investigation of the role of the last shear plane) and LP (investigation of the role of the penultimate shear plane).

It should be noted that the crack growth curves of the route-8B_C UFG IF steel are very similar in both the Paris regime and the near-threshold region (Fig. 4). Even though crack growth in the samples cut along three different orientations not perpendicular to the loading direction was monitored (Figs. 4 and 5), the deviation from the expected crack growth direction is quite similar in all cases, with slightly larger inclinations for the FP and LP samples. Therefore, the crack growth rates in FP and LP specimens are slightly higher upon correction.

In addition, crack growth always occurs in a direction parallel to the last ECAP shear plane, leading to the conclusion that the ECAP shear plane has a deteriorating influence on the crack growth behavior, even for an optimized ECAP route. Specifically, in terms of crack propagation direction, the role of sample orientation is more pronounced for the route-2A UFG IF steel (Fig. 4). The higher crack growth rates and the lower fatigue threshold values were observed for the FP samples in general, but the variation was much more pronounced in this material (Fig. 4). For the TP samples of 2A material, crack growth was perpendicular to the loading direction, but in FP samples, crack growth was similar to the behavior in the route-8B_C samples. So in the case of non-optimized ECAP processing the elongated microstructure, which has been described in former studies [16, 33, 34], features a mechanical behavior dependent on sample orientation with respect to the loading direction [35].

Crack growth–microstructure relationship

The crack growth behavior depicted in high magnification is presented in Fig. 5. The SEM images in the upper part of Fig. 5, and Figs. 6 and 7 show a step-like crack growth behavior in route-8B_C UFG IF steel samples in two different orientations (FP and TP). The surface of the FP sample shows bifurcations, which lead to deflections of the crack growth direction, and the surface of the TP sample shows pronounced step-like structures, again leading to deviation from the original direction of crack growth (Fig. 5). This step-like structure of crack advance clearly indicates that the deviation in the crack growth direction in UFG steel is not caused by a deteriorated shear strength of the material, but by microstructural features, such as elongated grains.

The micrograph presented in the lower part of Fig. 5 shows the surface topography of a route-8B_C FP sample. The plastic zone in the crack wake is clearly visible, the thickness of the sample is slightly decreased in this area, leading to a lower topography level in the CMS plot, and there is a kinked area characterized by a higher level topography. The presence of extrusions after fatigue loading, which stem from microstructural imperfections, such as large areas dominated by LAGBs and elongated structures, has already been shown for UFG samples in the LCF regime [33, 34]. In the current route-2A material, the crack obviously follows the elongated grain structures, which are an agglomeration of subgrains only divided by LAGBs (Fig. 6). This finding holds true for the route-8B_C UFG IF steel, as well. However, it is not seen as clearly due to the optimized processing and the corresponding lower degree of elongation. As can be deduced primarily from the EBSD map shown for the route-2A material, the elongated structures are ordered in a parallel fashion, dictating the direction of crack growth. Kinking is only observed in areas featuring grain structures with more equiaxed shapes and different misorientations.

It has been previously shown that elongated grain structures play a dominant role in the crack initiation processes [34]. Specifically, the locally increased stresses induced by the elongated grains in the matrix dictate the crack initiation sites. Similarly, in the case of crack advance, this stress rising effect along elongated structures drives the crack growth process (Fig. 6). These structures are preferentially ordered along the direction of material flow during ECAP [2, 26], and therefore, the influence of the last ECAP shear planes is pronounced (visible on FP and LP, c.f. Figs. 4, 5, and 6). Currently, the role of defects, i.e., micro pores [36], introduced during ECAP processing on the crack growth behavior and the reason for the unusual crack growth behavior on TP in route-8B_C and 16E materials are still unexplored, and work is underway to clarify these issues.

Finally, a careful evaluation of the current results provides important guidelines regarding the role of ECAP processing on the microstructure–fatigue crack propagation, overall fatigue performance relationship. A strong relationship between sample orientation and crack deflection has already been observed in fracture toughness

measurements conducted on UFG HPT Armco iron, where elongated structures were also observed [37]. The schematic presented in Fig. 9 summarizes the current findings obtained from samples on the FP, and accordingly, the crack growth behavior is very sensitive to ECAP processing. Specifically, in its CG state, the IF steel samples exhibit the best resistance against crack propagation, even though they exhibit poor crack initiation and overall fatigue lives [16]. A similar trend is valid for the UFG variants obtained by non-optimized ECAP processing, where the overall fatigue performance is better than that of the CG material [16, 33]. In the case of UFG IF steel obtained by optimized ECAP processing, however, the crack growth rates are the highest (Fig. 9), despite the superior fatigue performance and longest crack initiation periods [16, 33].

The current microstructural findings indicate that the microstructure dictates this behavior, such that the grain shape and grain misorientation become of utmost importance. The elongated grain structures drive the crack away from the expected direction, mainly due to added stress concentration they impose upon the matrix (Fig. 9). These elongated grain structures feature a large volume fraction of LAGBs, and thus, the crack progresses along the direction the LAGBs are cut through, i.e., along the major axes of the grains. As for the UFG material obtained upon optimized ECAP processing, the regularly shaped grains are divided mainly by HAGBs; yet, the already large stress concentration aids the crack growth. Furthermore, as the crack approaches these zones a deviation of the crack from the initial propagation direction is observed (Fig. 9). This, however, is absent in the CG material, and the crack paths in UFG materials are less tortuous, and roughness-induced crack closure is not as pronounced as in the CG counterparts.

Conclusions

The role of ECAP on the crack growth behavior in UFG IF steel was investigated. Miniature compact tension specimens extracted from IF steel processed along several ECAP routes with different order of material flow during ECAP processing were used to evaluate both crack growth rates as a function of loading amplitude and direction of crack growth. Mechanical testing was accompanied by thorough microstructural investigations using scanning electron microscopy, confocal laser scanning microscopy, and electron backscatter diffraction. The following conclusions can be drawn from the work presented herein:

1. Crack growth rates increase and fatigue threshold values decrease concomitant with decreasing grain size in UFG IF steel. The fatigue threshold value decreases by a factor of two comparing coarse-grained and route-$8B_C$ UFG materials.
2. The ECAP processing route significantly influences the crack advance. Specifically, a significant deviation from the expected direction of crack growth normal to the loading direction is notable, where the deviation from the normal direction is a function of the ECAP processing route.
3. Sample orientation is another factor dictating the crack advance. Direction of crack growth on flow and longitudinal planes depends on the ECAP shear plane in all UFG IF steel variants.

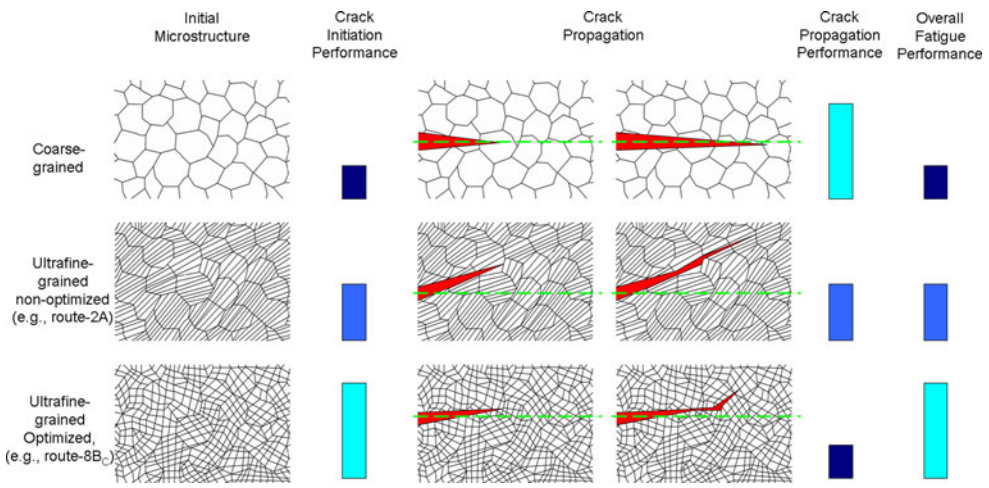

Fig. 9 Schematic summarizing the microstructure–crack propagation–overall fatigue performance relationship in UFG IF steel. Samples on the FP are considered. The dashed line indicates the expected crack propagation direction. The bars schematically represent the relative crack initiation, crack propagation, and overall fatigue performances of different microstructures. The weak microstructural alignment in the route-$8B_C$ material (Fig. 6) has been omitted in the schematic

4. Overall, the microstructure induced upon ECAP processing dictates the crack growth behavior. In particular, in the case of crack propagation, elongated structures oriented parallel to the direction of material flow during ECAP processing form local stress fields that direct the crack as it grows.

Acknowledgements The help of B. Gorny with CSM is acknowledged. The German part of this study was supported by Deutsche Forschungsgemeinschaft, within the Research Unit Program "Mechanische Eigenschaften und Grenzflächen ultrafeinkörniger Werkstoffe." The U.S. part of this study was supported by the National Science Foundation, contract no. CMMI-0900187, Materials and Surface Engineering Program, Directorate of Engineering, Arlington, VA.

References

1. Segal VM (1995) Mater Sci Eng A197:157
2. Valiev RZ, Langdon TG (2006) Progr Mater Sci 51:881. doi:10.1016/j.pmatsci.2006.02.003
3. Valiev RZ, Korznikov AV, Mulyukov RR (1993) Mater Sci Eng A A168:141
4. Meyers MA, Mishra A, Benson DJ (2006) Progr Mater Sci 51:427. doi:10.1016/j.pmatsci.2005.08.003
5. Gleiter H (1989) Progr Mater Sci 33:233
6. Valiev RZ, Alexandrov IV, Zhu YT, Lowe TC (2002) J Mater Res 17:5
7. Valiev RZ, Estrin Y, Horita Z, Langdon TG, Zehetbauer MJ, Zhu YT (2006) JOM 58:33. doi:10.1007/s11837-006-0213-7
8. Koch CC, Youssef KM, Scattergood RO, Murty KL (2005) Adv Eng Mater 7:787. doi:10.1002/adem.200500094
9. Zhilyaev AP, Nurislamova GV, Kim BK, Baró MD, Szpunar JA, Langdon TG (2003) Acta Mater 51:753. doi:10.1016/S1359-6454(02)00466-4
10. Höppel HW, May J, Göken M (2004) Adv Eng Mater 6:781. doi:10.1002/adem.200306582
11. Zhu YT, Lowe TC (2000) Mater Sci Eng A291:46. doi:10.1016/S0921-5093(00)00978-3
12. Kawasaki M, Horita Z, Langdon TG (2009) Mater Sci Eng A524:143. doi:10.1016/j.msea.2009.06.032
13. Semenova LP, Valiev RZ, Yakushina EB, Salimgareeva GH, Lowe TC (2008) J Mater Sci 43:7354. doi:10.1007/s10853-008-2984-4
14. Niendorf T, Canadinc D, Maier HJ, Karaman I (2009) Scripta Mater 60:344. doi:10.1016/j.scriptamat.2008.10.033
15. Shin DH, Park KT (2005) Mater Sci Eng A410–411:299. doi:10.1016/j.msea.2005.08.025
16. Niendorf T, Canadinc D, Maier HJ, Karaman I, Sutter SG (2006) Int J Mater Res 97:1328
17. Vinogradov A (2007) J Mater Sci 42:1797. doi:10.1007/s10853-006-0973-z
18. Mughrabi H, Höppel HW (in press) Int J Fat. doi:10.1016/j.ijfatigue.2009.10.007
19. Kim HK, Choi MI, Chung CS, Shin DH (2003) Mater Sci Eng A340:243
20. Niendorf T, Canadinc D, Maier HJ, Karaman I (2008) Int J Fatigue 30:426. doi:10.1016/j.ijfatigue.2007.04.015
21. Segal VM, Goforth RE, Hartwig KT (1995) Texas A&M University, U.S. Patent No. 5,400,633
22. Barber RE, Dudo T, Yasskin PB, Hartwig KT (2004) Scripta Mater 51:373. doi:10.1016/j.scriptamat.2004.05.022
23. ASTM Standard E 647-08, American society for testing and materials
24. Sander M, Richard HA (2006) Int J Fat 28:583. doi:10.1016/j.ijfatigue.2005.05.012
25. Niendorf T, Rubitschek F, Maier HJ, Niendorf J, Richard HA, Frehn A (2010) Mater Sci Eng A527:2412. doi:10.1016/j.msea.2009.12.012
26. May J (2008) Dissertation, University of Erlangen-Nuremberg
27. May J, Dinkel M, Amberger D, Höppel HW, Göken M (2007) Metall Mater Trans 38A:1941. doi:10.1007/s11661-007-9110-0
28. Hübner P, Kiessling R, Biermann H, Hinkel T, Jungnickel W, Kawalla R, Höppel HW, May J (2007) Metall Mater Trans 38A:1926. doi:10.1007/s11661-007-9297-0
29. Meyer LW, Sommer K, Halle T, Hockauf M (2008) J Mater Sci 43:7426. doi:10.1007/s10853-008-2725-8
30. Vinogradov A, Nagasaki S, Patlan V, Kitagawa K, Kawazoe M (1999) Nano Struc Mater 11:925. doi:10.1016/S0965-9773(99)00392-X
31. Elber W (1970) Eng Fract Mech 2:37
32. Suresh S (1998) Fatigue of materials. University Press, Cambridge, UK
33. Niendorf T, Canadinc D, Maier HJ, Karaman I (2007) Metall Mater Trans 38A:1946. doi:10.1007/s11661-007-9154-1
34. Niendorf T, Dadda J, Canadinc D, Maier HJ, Karaman I (2009) Mater Sci Eng A517:225. doi:10.1016/j.msea.2009.04.053
35. Niendorf T, Marten T, Maier HJ, Karaman I (2008) Mater Sci For 584–586:864
36. Lapovok R, Tomus D, Mang J, Estrin Y, Lowe TC (2009) Acta Mater 57:2909. doi:10.1016/j.actamat.2009.02.042
37. Hohenwarter A, Pippan R (2010) Mater Sci Eng A527:2649. doi:10.1016/j.msea.2009.12.033